ChemComm

Accepted Manuscript

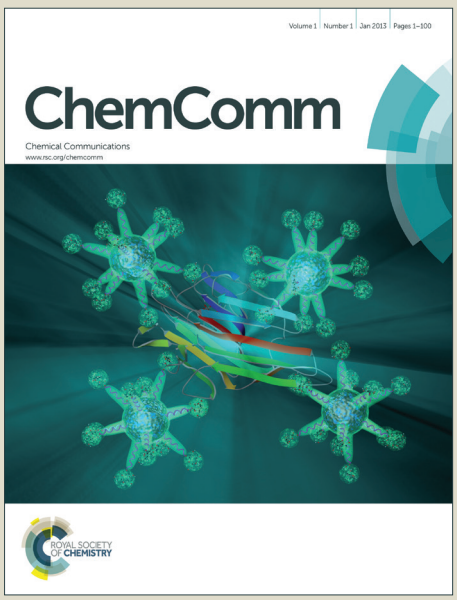

ROYAL SOCIETY OF CHEMISTRY

www.rsc.org/chemcomm

Journal Name

RSCPublishing

COMMUNICATION

In-situ Growth of $MoSe_2$/Mo Counter Electrode for High Efficiency Dye-sensitized Solar Cells

Cite this: DOI: 10.1039/x0xx00000x

Haijie Chen,‡[a,b] Yian Xie,‡[a,b] Houlei Cui,[a] Wei Zhao,[a] Xiaolong Zhu,[a] Yaoming Wang,[a] Xujie Lü,[c] and Fuqiang Huang[a,b,*]

Received 00th January 2012,
Accepted 00th January 2012

DOI: 10.1039/x0xx00000x

www.rsc.org/

A facile and economical $MoSe_2$/Mo structure was in-situ prepared to replace the currently preferred expensive Pt and FTO counter electrode (CE) in dye-sensitized solar cells. A power conversion efficiency of 8.13% was achieved, comparable to that with Pt-sputtered FTO electrode (8.06%).

A dye-sensitized solar cell (DSSC) is typically composed of dye-coated nanocrystalline TiO_2 electrode on fluorine-doped SnO_2 (FTO), electrolyte containing the triiodide/iodide redox couple (I_3^-/I^-) and counter electrode (CE). The CE is responsible for transferring electrons from the external circuit to the electrolyte and catalyzing the reduction of I_3^- to I^- in the electrolyte. The conventional CE is a F-doped tin oxide (FTO) glass coated with Platinum (Pt) electrocatalyst, which contributes to a major share of the cost in preparation.[1,2] In order to promote the commercialization of DSSCs, it is necessary to explore alternative materials to replace Pt and FTO with low-cost and high-efficiency.

Many candidates have been proposed to replace Pt, such as carbonaceous materials,[3,4] metal oxides,[5,6] sulfides,[7-13] nitrides,[14,15] *etc*.[16] Recently, the selenides have also been proved to be excellent choices.[17-19] $MoSe_2$, one of the important transition metal selenides, is a narrow-band gap semiconductor with a lamellar crystal structure, which has been applied in solar cells and photocatalysis.[20-22] $MoSe_2$ has never been introduced into DSSCs as a CE material. On the other hand, in the previous reports, several methods were introduced to prepare CEs, such as spin-coating,[3] drop-casting,[12] electrochemical depositon,[15,17] *etc*. However, the fitted series resistance (R_s) of the CEs, related to the collection of electrons from the external circuit, is usually not low enough to obtain ideal fill factor (*FF*) as previously reported, which is partially because of the weak connection between electrocatalytic layer and the substrate.[23] It is highly desirable to explore other effective approach to prepare CE to obtain lower R_s for better photovoltaic performance.

In this paper, we proposed a facile and economical $MoSe_2$/Mo counter electrode. The top $MoSe_2$ layer functions as electrocatalytic center for I_3^- reduction, and the bottom Mo layer acts as conductive collector for electron extraction. The preparation is simple but effective via a strategy of in-situ selenization of Mo film on a glass substrate. This method formed a perfect Ohmic contact between the $MoSe_2$ layer and the Mo layer, generating small R_s. The superior electrocatalytic activity of $MoSe_2$ leads to low charge-transfer resistance (R_{ct}). As a result, the DSSC assembled with $MoSe_2$/Mo CE has higher *FF* and V_{oc} than that with Pt-sputtered FTO. The obtained power conversion efficiency (8.13%) is comparable to the latter (8.06%). Considering the requirement of selenization process in CIGSSe solar cell fabrication, we further successfully fabricated a bifacial solar cell with front CIGSSe cell and rear DSSC.

Mo thin films were firstly deposited onto the glass substrate by magnetron sputtering. As shown in Fig. 1a, Mo thin film shows fish scale shape (~100 nm). The electrical conductivity of the Mo film was measured by a standardized "four-point probe" setup in order to eliminate contact resistance. The Mo thin film provides a superior electrical conductivity of 28.1 $\mu\Omega$·cm. Then, the $MoSe_2$/Mo/Glass structure was obtained after annealing the Mo-coated glass substrate at 500 °C for 30 min in Se atmosphere. As shown in Fig. 1b, homogeneous and uniform surface was covered by small particles (~100 nm). The $MoSe_2$ layer was further scraped for transmission electron microscopy (TEM) measurement. The interlayer *d*-spacing between the lattice fringes determined to be 3.27 Å is assigned to be the (004) planar spacing (3.23 Å) of $MoSe_2$. Fig. 1c shows XRD patterns of the $MoSe_2$/Mo structure. The Mo substrate shows a preferred high orientation of the (110) plane, consistent to our former result.[24] The Mo peak remains after selenization, indicating partial selenization of the Mo layer, confirming $MoSe_2$/Mo bilayer structure. The (100) and (110) peaks of $MoSe_2$ are well indexed (JCPDS, PDF no. 29-0914).

The cross-sectional scanning electron microscopy (SEM) image is shown in Fig. 1d. A bilayer structure with 770 nm Mo and 558 nm $MoSe_2$ is presented. Fig. 1e shows the EDS line scan results along the perpendicular direction of the $MoSe_2$/Mo structure (Fig. S1 in the Supporting Information (SI)). No Se element was detected in the

bottom Mo layer. The Mo and Se distribute linearly along the scan direction in the transition region between the two layers, which demonstrates that the $MoSe_2$ layer is in intimate contact with the Mo layer. This result coincides well with the cross-sectional SEM results. The formation of $MoSe_2$/Mo structure generates Ohmic-type contact, which can be explained by the different work functions between the *p*-type $MoSe_2$ semiconductor (4.4 eV) and the Mo metal (4.6 eV).[25] For separate $MoSe_2$ and Mo, the Fermi level of the former is higher than the latter based on the same electronic vacuum energy level. In the $MoSe_2$/Mo bilayer structure where the two have intimate contact, their Fermi level reaches the same level. Herein, as shown in Fig. 2f, the energy band of the $MoSe_2$ semiconductor upsweeps. A highly conductive region is generated, which benefits charge transfer. It is easy for holes to transfer from $MoSe_2$ into Mo.

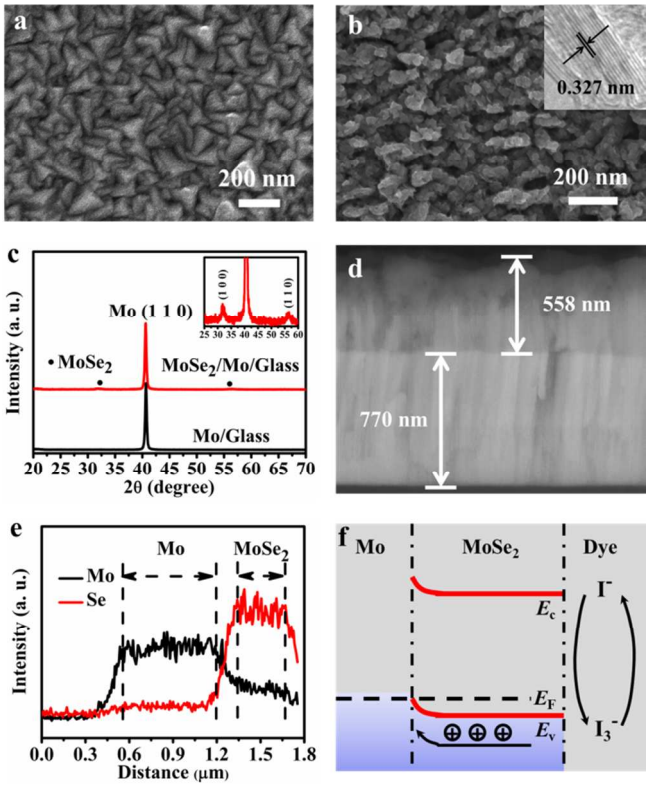

Fig. 1 (a) SEM top-view image of magnetron sputtered Mo thin film and (b) $MoSe_2$ layer (Inset: high-resolution TEM image of the synthesized $MoSe_2$), (c) XRD patterns of the $MoSe_2$/Mo structure with the Mo substrate as a reference (Inset: a magnification of the XRD pattern), (d) cross-sectional SEM image of the $MoSe_2$/Mo structure, (e) EDS line-scan profile of Mo and Se elements, and (f) illustration of the formation of Ohmic-type heterocontact in $MoSe_2$/Mo structure (E_F: Fermi level, E_c: bottom of the conduction band of $MoSe_2$, E_v: top of the valence band of $MoSe_2$).

The $MoSe_2$/Mo structure was used as CE to assemble the DSSC, as shown in Fig. 2a. The photovoltaic properties of DSSCs with $MoSe_2$/Mo and Pt/FTO CEs under the same illumination are displayed in Fig. 2b and also summarized in Table 1. The DSSC with $MoSe_2$/Mo CE produces an efficiency of 8.13% (J_{sc} = 15.07 mA cm^2, V_{oc} = 805 mV, and FF = 0.67), which is comparable to that with Pt/FTO CE (η = 8.06%; J_{sc} = 16.11 mA cm^2, V_{oc} = 794 mV, FF = 0.63). For comparison, the $MoSe_2$/Mo CEs have also been prepared for 10min and 60 min, respectively. The performances of the corresponding DSSCs are shown in Fig. S2 and S3 in the SI. The thinner layer leads to less $MoSe_2$, which is not sufficient for the reduction of I_3^-. Besides, due to the inherent resistance of $MoSe_2$, too thick layer is not beneficial for the transfer of the electron. So there is a tradeoff between the resistance of the $MoSe_2$ and the loading amounts of $MoSe_2$. The thickness of 558 nm is an optimal value for $MoSe_2$ layer in this study.

Table 1. Photovoltaic parameters of DSSCs based on $MoSe_2$/Mo and Pt-sputtered FTO CEs.

CEs	J_{sc} (mA cm^{-2})	V_{oc} (mV)	FF	η (%)	R_s (Ω)	R_{ct} (Ω)
$MoSe_2$/Mo	15.07	805	0.67	8.13	2.64	0.30
Pt	16.11	794	0.63	8.06	15.98	8.95

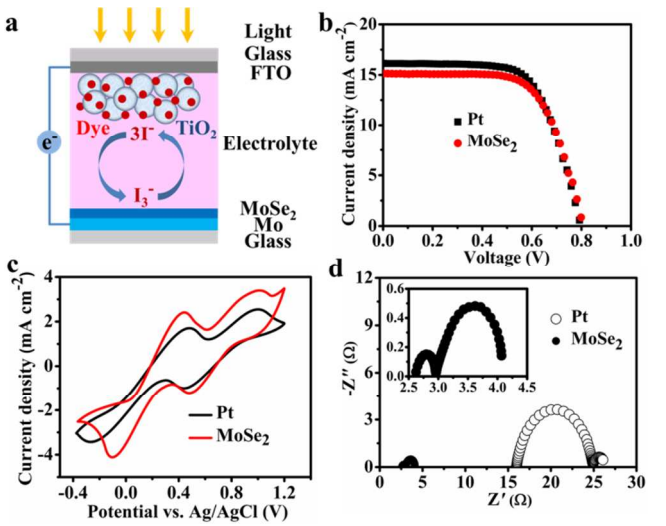

Fig. 2 (a) The deployment of $MoSe_2$/Mo structure as counter electrode (CE) in DSSC, (b) photovoltaic performances of DSSCs based on $MoSe_2$/Mo and Pt-sputtered FTO (Pt/FTO) CEs, (c) cyclic voltammograms of I^-/I_3^-, and (d) Nyquist plots of the symmetric cells.

This is the first investigation to report a $MoSe_2$/Mo CE in a DSSC. In order to evaluate the electrocatalytic activity , the cyclic voltammetry (CV) was measured in a three-electrode system. For comparison, CV of Pt electrode was also performed under the same condition. As shown in Fig. 2c, both CEs have typical curves with two pairs of redox peaks and two cathodic peaks,[10] which relate to the two-step process of I_3^- reduction denoted in Equations 1 and 2:

$$I_3^- + 2e^- \leftrightarrow 3I^- \quad (1)$$

$$3I_2 + 2e^- \leftrightarrow 2I_3^- \quad (2)$$

The similar shape of the curve for the $MoSe_2$/Mo structure as that of Pt/FTO results in similar electrochemical behavior. Furthermore, the $MoSe_2$/Mo eletrode exhibits higher current density, which reveals a much faster catalytic rate towards the I_3^-/I^- redox couple. $MoSe_2$ is an excellent choice to replace the expensive Pt in DSSC.

In order to further evaluate the electrochemical characteristics, the electrochemical impedance spectra (EIS) measurements were carried out using symmetric cells fabricated with two identical electrodes (CE/electrolyte/CE). The obtained Nyquist plots conducted in the dark without bias potential were illustrated in Fig. 2d. Two semicircles in the

high and low-frequency regions are observed for all the CEs. The intercept of the semicircle in the high-frequency region on the real axis is assigned to the ohmic series resistance (R_s). The semicircle in the high-frequency range of the Nyquist plot is related to the charge-transfer resistance (R_{ct}) of I_3^- reduction.[23,26] R_s and R_{ct} are evaluated by fitting the impedance spectra with the equivalent circuit (Fig. S4 in the SI) using the Zview software. The R_s is related to the collection of electrons from the external circuit. Generally, R_s increases with the surface area of the CE and is reversely proportional to the *FF*.[27,28] As listed in Table 1, the obtained R_s value of $MoSe_2$/Mo CE (2.64 Ω) is only 16.5% of Pt/FTO (15.98 Ω). R_{ct}, crucial to the electron transfer, is correlated with the interface between electrolyte and CE. R_{ct} of $MoSe_2$/Mo CE is (0.30 Ω) is 3.35% of Pt/FTO (8.95 Ω), further indicating superior electrocatalytic activity of $MoSe_2$ for the reduction of I_3^-.

Bifacial solar cell, which can converts light into electricity at both sides of the cell, is also an economical choice and has promising applications.[29,30] The selenization process is an improtant process in fabricating CIGSSe solar cells. The application of $MoSe_2$/Mo structure as CE in DSSC makes possible a bifacial cell consisting of CIGSSe solar cell as front cell for absorbing intense sunlight and DSSC as rear one for weak irradiation. Mo was sputtered onto both sides of the glass substrate followed by selenization. After this, one side was for CIGSSe cell and the other was for DSSC. A bifacial solar cell was sucessfully fabricated (Fig. S5 in the SI).

Conclusions

In summary, sputtered Mo on glass substrates was in-situ selenized to synthesize $MoSe_2$/Mo bilayer structure. The obtained $MoSe_2$/Mo electrode was successfully introduced into DSSC as CE to substitute expensive Pt/FTO electrode. CV and EIS measurements demonstrate superior electrocatalytic activity for $MoSe_2$/Mo structure towards the reduction of I_3^-. A power conversion efficiency of 8.13% was obtained, which is comparable to that with Pt-sputtered FTO (8.06%). Due to this application, we further successfully fabricated a bifacial solar cell with front CIGSSe cell and rear DSSC.

This work was financially supported by National 863 Program of China (Grant No. 2011AA050505), NSF of China (Grants Nos. 51125006, 91122034, 51202279, 61376056), and Science and Technology Commission of Shanghai (Grant No. 12XD1406800).

Notes and references

[a] *CAS Key Laboratory of Materials for Energy Conversion and State Key Laboratory of High Performance Ceramics and Superfine Microstructures, Shanghai Institute of Ceramics, Chinese Academy of Sciences, Shanghai 200050, People's Republic of China. Email: huangfq@mail.sic.ac.cn; Tel: +86-21-52416360.*

[b] *State Key Laboratory of Rare Earth Materials Chemistry and Applications, College of Chemistry and Molecular Engineering, Peking University, Beijing 100871, People's Republic of China*

[c] *High Pressure Science and Engineering Center (HiPSEC), University of Nevada, Las Vegas, Nevada 89154, USA*

† Electronic Supplementary Information (ESI) available: [details of any supplementary information available should be included here]. See DOI: 10.1039/c000000x/

‡ Haijie Chen and Yian Xie contributed equally to this work.

1. B. E. Hardin, H. J. Snaith and M. D. McGehee, *Nat. Photonics*, 2012, **6**, 162.
2. K. S. Lee, H. K. Lee, D. H. Wang, N. G. Park, J. Y. Lee, O. O. Park and J. H. Park, *Chem. Commun.*, 2010, **46**, 4505.
3. J. D. Roy-Mayhew, D. J. Bozym, C. Punckt and I. A. Aksay, *ACS nano*, 2010, **4**, 6203.
4. B. Lee, D. B. Buchholz and R. Chang, *Energy Environ. Sci.*, 2012, **5**, 6941.
5. M. X. Wu, X. Lin, A. Hagfeldt and T. L. Ma, *Chem. Commun.*, 2011, **47**, 4535.
6. X. Lin, M. X. Wu, Y. D. Wang, A. Hagfeldt and T. L. Ma, *Chem. Commun.*, 2011, **47**, 11489.
7. J. Yang, C. X. Bao, J. Y. Zhang, T. Yu, H. Huang, Y. L. Wei, H. Gao, G. Fu, J. G. Liu, and Z. G. Zou, *Chem. Commun.*, 2013, **49**, 2028.
8. X. J. Zheng, J. H. Guo, Y. T. Shi, F. Q. Xiong, W. H. Zhang, T. L. Ma, and C. Li, *Chem. Commun.*, 2013, **49**, 9645.
9. C. W. Kung, H. W. Chen, C. Y. Lin, K. C. Huang, R. Vittal and K. C. Ho, *ACS nano*, 2012, **6**, 7016.
10. M. K. Wang, A. M. Anghel, B. Marsan, N. L. Cevey Ha, N. Pootrakulchote, S. M. Zakeeruddin and M. Grätzel, *J. Am. Chem. Soc.*, 2009, **131**, 15976.
11. W. Zhao, T. Q. Lin, S. R. Sun, H. Bi, P. Chen, D. Y. Wan, and F. Q. Huang, *J. Mater. Chem. A*, 2013, **1**, 194.
12. X. K. Xin, M. He, W. Han, J. H. Jung and Z. Q. Lin, *Angew. Chem. Int. Ed.*, 2011, **50**, 11739.
13. L. X. Yi, Y. Y. Liu, N. L. Yang, Z. Y. Tang, H. J. Zhao, G. H. Ma, Z. G. Su, and D. Wang, *Energy Environ. Sci.*, 2013, **6**, 835.
14. Q. W. Jiang, G. R. Li and X. P. Gao, *Chem. Commun.*, 2009, 6720.
15. G. R. Li, J. Song, G. L. Pan and X. P. Gao, *Energy Environ. Sci.*, 2011, **4**, 1680.
16. Y. Y. Dou, G. R. Li, J. Song and X. P. Gao, *Phys. Chem. Chem. Phys.*, 2012, **14**, 1339.
17. F. Gong, H. Wang, X. Xu, G. Zhou and Z. S. Wang, *J. Am. Chem. Soc.*, 2012, **134**, 10953.
18. F. Gong, X. Xu, Z. Q. Li, G. Zhou and Z. S. Wang, *Chem. Commun.*, 2013, **49**, 1437.
19. J. H. Guo, Y. T. Shi, C. Zhu, L. Wang, N. Wang, and T. L. Ma, *J. Mater. Chem. A*, 2013, **1**, 11874.
20. Y. F. Shi, C. X. Hua, B. Li, X. P. Fang, C. H. Yao, Y. C. Zhang, Y. S. Hu, Z. X. Wang, L. Q. Chen, D. Y. Zhao, and G. D. Stucky, *Adv. Funct. Mater.*, 2012, **23**, 1832.
21. L. F. Schneemeyer and M. S. Wrighton, *J. Am. Chem. Soc.*, 1980, **102**, 6964.
22. V. Pathak, K. Patel, R. Pathak and R. Srivastava, *Sol. Energy Mater. Sol. Cells*, 2002, **73**, 117.
23. Q. Wang, J. E. Moser and M. Grätzel, *J. Phys. Chem. B*, 2005, **109**, 14945.
24. X. L. Zhu, Z. Zhou, Y. M. Wang, L. Zhang, A. M. Li and F. Q. Huang, *Sol. Energy Mater. Sol. Cells*, 2012, **101**, 57.
25. T. Shimada, F. S. Ohuchi and B. A. Parkinson, *Jpn. J. Appl. Phys.*, 1994, **33**, 2696.
26. M. X. Wu, X. Lin, A. Hagfeldt and T. L. Ma, *Angew. Chem. Int. Ed.*, 2011, **50**, 3520.

27. N. Koide, A. Islam, Y. Chiba and L. Han, *J. Photochem. Photobiol. A*, 2006, **182**, 296.
28. X. J. Lü, X. L. Mou, J. J. Wu, D. W. Zhang, L. L. Zhang, F. Q. Huang, F. F. Xu and S. M. Huang, *Adv. Func. Mater.*, 2010, **20**, 509.
29. T. Uematsu, K. Tsutsui, Y. Yazawa, T. Warabisako, I. Araki, Y. Eguchi and T. Joge, *Sol. Energy Mater. Sol. Cells*, 2003, **75**, 557.
30. A. Hubner, A. G. Aberle and R. Hezel, *Appl. Phys. Lett.*, 1997, **70**, 1008.